ELSEVIER

Journal of Economic Behavior & Organization
Vol. 49 (2002) 173–197

JOURNAL OF
Economic Behavior
& Organization

www.elsevier.com/locate/econbase

Speculative behaviour and complex asset price dynamics: a global analysis

Carl Chiarella [a,*], Roberto Dieci [b], Laura Gardini [c]

[a] *School of Finance and Economics, University of Technology, P.O. Box 123, Sydney, NSW 2007, Australia*
[b] *Facoltà di Economia, Università degli Studi di Parma, Parma, Italy*
[c] *Facoltà di Economia, Università degli Studi di Urbino, Urbino, Italy*

Received 9 April 2001; received in revised form 16 July 2001; accepted 19 July 2001

Abstract

This paper analyses the dynamics of a model of a share market consisting of two groups of traders: fundamentalists, who base their trading decisions on the expectation of a return to the fundamental value of the asset, and chartists, who base their trading decisions on an analysis of past price trends. The model is reduced to a two-dimensional map whose global dynamic behaviour is analysed in detail. The dynamics are affected by parameters measuring the strength of fundamentalist demand and the speed with which chartists adjust their estimate of the trend to past price changes. The parameter space is characterized according to the local stability/instability of the equilibrium point as well as the non-invertibility of the map. The method of critical curves of non-invertible maps is used to understand and describe the range of global bifurcations that can occur. It is also shown how the knowledge of deterministic dynamics uncovered here can aid in understanding the behaviour of stochastic versions of the model.

JEL classification: C61; D84; G12

Keywords: Heterogeneous agents; Complex dynamics; Global dynamics; Non-invertible maps; Volatility clustering; Speculation

1. Introduction

In recent years several models of financial markets based on interacting heterogeneous agents have been developed, see for example Day and Huang (1990), Brock and Hommes (1998), Lux (1998), Chen and Yeh (1997) and Chiarella and He (in press). Most of these

* Corresponding author. Tel.: +61-2-9514-7719; fax: +61-2-9514-7711.
E-mail addresses: carl.chiarella@uts.edu.au (C. Chiarella), roberto.dieci@unipr.it (R. Dieci), gardini@econ.uniurb.it (L. Gardini).

0167-2681/02/$ – see front matter
PII: S0167-2681(02)00066-5

models, some of which allow the size of the different groups of agents to vary according to the evolution of the financial market, are of necessity not very mathematically tractable. In the present paper, in order to complement the aforementioned studies, we develop a discrete time model of asset price dynamics containing the essential elements of the heterogeneous interacting agents paradigm whilst still remaining mathematically tractable. We assume that the share market consists of two types of traders: *fundamentalists*, who base their trading decisions on an estimate of the fundamental value of the asset, and *chartists*, a group which bases its decisions on an analysis of past price trends. The chartists' demand is an S-shaped function of the difference between the chartists' estimate of the price trend (obtained through an adaptive expectations scheme on past price changes) and the return on some alternative asset. The model reduces to a two-dimensional non-linear map, whose dynamic behaviour we analyse by first determining, in the space of the parameters, the local stability region of the unique equilibrium point of the map, together with the regions of invertibility or non-invertibility. It turns out that in the stability region, besides the local properties, global ones are also important in detecting other dynamic phenomena such as coexistence of attractors, or chaotic transients before the convergence to the stable equilibrium. We indicate the bifurcations that the fixed point undergoes when the key parameters, such as the *strength* of fundamentalists' demand and the *speed* with which chartists adjust their estimate of the trend to past price changes, are increased. We also analyze the regions in the parameter space in which the equilibrium point is unstable and the map is non-invertible. We shall focus on particular regimes characterized by chaotic behaviour, showing how the global bifurcation known as *snap-back repellor* (leading to chaotic dynamics) can be detected by use of the *critical curves* of the map (as proved in Gardini (1994)). Moreover, by making use of the properties of the critical curves of non-invertible maps (described in Chapter 4 of Mira et al. (1996), and used in several economic models by Puu (2000)), we show how upper and lower bounds for the asymptotic behaviour of the state variables (price and chartists' expectations) can be determined, although we are in the presence of chaotic dynamics. Simulations of a stochastic version of the model suggest that volatility behaviour of asset returns is related to these bounds.

The paper is organized as follows. Section 2 derives the model of fundamentalists and chartists. Section 3 points out some general properties of the two-dimensional map driving the dynamics. Sections 4 discusses the bifurcations that can occur and Section 5 shows how the properties of the critical curves can help to understand the nature of the attractors, their homoclinic bifurcations and other global bifurcations. Finally, an extension of the model beyond its deterministic structure is suggested in Section 6, showing how the knowledge of deterministic dynamics can help in understanding the volatility patterns of simple stochastic versions of the model. Section 7 concludes and makes some suggestions for future research.

2. The model

We adopt the basic fundamentalist/chartist model of Chiarella (1992), whose antecedents are Day and Huang (1990), Beja and Goldman (1980), and Zeeman (1974). We denote by P_t the logarithm of the asset price at time t and use the subscript $i \in \{f, c\}$ to denote

fundamentalists or chartists. In each time period each group of agents is assumed to invest some of its wealth in a risky asset and some in an alternative safe asset. Let $\Omega_{i,t}$ be the wealth of agent i and $Z_{i,t}$ be the fraction of this wealth that agent i decides to invest in the risky asset, at time t. The agent's wealth at time $(t+1)$ will then be given by

$$\Omega_{i,t+1} = \Omega_{i,t} + \Omega_{i,t}(1 - Z_{i,t})g_t + \Omega_{i,t}Z_{i,t}(P_{t+1} - P_t),$$

where g_t is the return on the alternative safe asset (e.g. bonds) and $(P_{t+1} - P_t)$ is the return on the risky asset. Agent i computes the conditional mean and variance of $\Omega_{i,t+1}$ (denoted by $E_{i,t}(\Omega_{i,t+1})$ and $V_{i,t}(\Omega_{i,t+1})$, respectively) assuming that $(P_{t+1} - P_t)$ is conditionally normal, so that

$$E_{i,t}(\Omega_{i,t+1}) = \Omega_{i,t} + \Omega_{i,t}(1 - Z_{i,t})g_t + \Omega_{i,t}Z_{i,t}E_{i,t}(P_{t+1} - P_t), \tag{1}$$

$$V_{i,t}(\Omega_{i,t+1}) = Z_{i,t}^2\Omega_{i,t}^2V_{i,t}(P_{t+1} - P_t). \tag{2}$$

Assuming that each group of agents has an exponential utility of wealth function, each agent seeks $Z_{i,t}$ so as to maximise

$$E_{i,t}[-\exp(-\alpha_i\Omega_{i,t+1})], \tag{3}$$

where α_i is agent i's risk aversion coefficient. Under the assumption that $\Omega_{i,t+1}$ is conditionally normally distributed, this problem is equivalent to

$$\max_{Z_{i,t}} \left\{ E_{i,t}(\Omega_{i,t+1}) - \frac{1}{2}\alpha_i V_{i,t}(\Omega_{i,t+1}) \right\}.$$

The solution to this optimization problem is

$$\zeta_{i,t} \equiv Z_{i,t}\Omega_{i,t} = \frac{E_{i,t}(P_{t+1} - P_t) - g_t}{\alpha_i V_{i,t}(P_{t+1} - P_t)},$$

where $\zeta_{i,t}$ is the demand by agent i for the risky asset. The two groups of agents essentially differ in the way they calculate the mean and variance of the price change over successive time intervals.

The fundamentalists are assumed to have a reasonable estimate of the fundamental value of the risky asset. This estimate has been obtained at some cost, such as large setup costs (e.g. a major financial institution), and the employment of highly paid professionals, such as market analysts, economists, computer analysts, etc. Fundamentalists believe that the asset price follows a mean reversion process with the fundamental value being the long run mean. Hence they calculate that the expected excess return is proportional to the difference between the current log asset price and the log fundamental value, i.e.

$$E_{\mathrm{f},t}(P_{t+1} - P_t) - g_t = \eta(W_t - P_t),$$

where η is the speed of mean reversion estimated by the fundamentalists and W_t is the log of fundamental value at time t. They also assume that the conditional variance of price changes is constant, i.e.

$$V_{\mathrm{f},t}(P_{t+1} - P_t) = v_{\mathrm{f}}.$$

Fundamentalist demand, in terms of returns, is thus given by

$$D_t^{\mathrm{f}} = a(W_t - P_t), \tag{4}$$

where a ($= \eta/\alpha_{\mathrm{f}} v_{\mathrm{f}} > 0$) is the strength of fundamentalist demand. If the log share price P_t is below (above) the log expected fundamental value W_t, then fundamentalists try to buy (sell) the share, because they think that the share is undervalued (overvalued) and therefore its price will increase (decrease).

Chartists are assumed to be unable to bear the cost structure necessary to acquire the information about the fundamental value available to fundamentalists. Rather they base their estimate of the mean and variance of expected return on the risky asset on the costless information contained in recent return (log price) changes.[1] Use $\psi_{t,t+1}$ to denote the chartists' expectation at time t of the log price change (i.e. return) over the next trading period, i.e.

$$\psi_{t,t+1} = E_t(P_{t+1} - P_t) = E_t(P_{t+1}) - P_t.$$

Then chartists are assumed to calculate $E_{\mathrm{c},t}(P_{t+1} - P_t)$ by extrapolating past price changes according to the simple adaptive scheme

$$\psi_{t,t+1} = \psi_{t-1,t} + c(P_t - P_{t-1} - \psi_{t-1,t}), \tag{5}$$

where c ($0 < c \leq 1$) is the speed with which they adjust their estimate of the trend to the most recent price changes. Alternatively the quantity $\tau = 1/c$ may be viewed as the time lag in chartists' information.[2]

Thus, chartist asset demand is given by

$$\zeta_{\mathrm{c},t} = \frac{\psi_{t,t+1} - g_t}{\alpha_{\mathrm{c}} v_{\mathrm{c}}}.$$

Unlike the fundamentalists, the chartists change their estimate v_{c} of the conditional variance according to the magnitude of $|\psi_{t,t+1} - g_t|$. As this quantity becomes larger they expect greater volatility and increase their estimate v_c, hence lowering the slope of their demand function. This behaviour leads to the levelling off of the slope of chartist demand as $|\psi_{t,t+1} - g_t|$ becomes larger. The chartist asset demand may thus be characterised in general by

$$D_t^{\mathrm{c}} = h(\psi_{t,t+1} - g_t), \tag{6}$$

where the function $h(\cdot)$ has the properties: (i) $h'(x) > 0$ $(\forall x)$, (ii) $h(0) = 0$, (iii) there exists an x^* such that $h''(x) < 0$ (> 0) for all $x > x^*$ $(< x^*)$ and, (iv) $\lim_{x \to \mp\infty} h'(x) = 0$. In our examples and simulations we take $h(x) = \gamma \arctan x$. However, it is important to remark that the qualitative analysis performed in the following sections (as also the qualitative dynamics) are not affected by a change of function, because these mainly depend on the properties of $h(\cdot)$ given above.

[1] Alternatively we could conceive of chartists as a group having greater faith in the statistical analysis of recent price trends than in attempts to estimate fundamental value.

[2] The restriction $c \leq 1$, i.e. $\tau \geq 1$, has the simple economic interpretation that chartists cannot revise their estimate of $\psi_{t,t+1}$ more frequently than they receive information about price changes. Here this frequency is one time unit.

Thus, total excess demand for the asset at time t (assuming $g_t = g$ and $W_t = W$ are both constant) is given by

$$D_t = a(W - P_t) + h(\psi_{t,t+1} - g). \tag{7}$$

Let us now turn to the adjustment process of the share price in the market. Following Day and Huang, we assume the existence of a *market maker* whose function is to set excess demand to zero at the end of each trading day. If the excess demand in period t is positive (negative), the market maker sells (buys) the quantity of the asset needed to clear the market, and raises (reduces) the share price for the next period $t + 1$. Precisely, what goes on in each trading day can be described as follows: (i) at the beginning of day t the market maker announces the (log) price P_t for that day; (ii) the market participants then form excess demand D_t according to (7); (iii) the market maker, observing the excess demand, takes a long or short position M_t (by adjusting his or her inventory of assets) in order to clear the market, i.e. such that $D_t + M_t = 0$; (iv) the market maker then announces, at the beginning of the next trading period, the new (log) price P_{t+1} calculated as the previous (log) price plus some fraction of the excess demand of the previous period, according to $P_{t+1} = P_t + \beta_p D_t$ ($\beta_p > 0$). The process then repeats itself.[3]

Thus, at the beginning of day $(t + 1)$ the following dynamic adjustments occur, made by the market maker and chartists, respectively:

$$\begin{cases} P_{t+1} = P_t + \beta_p[a(W - P_t) + h(\psi_{t,t+1} - g)], \\ \psi_{t+1,t+2} = (1 - c)\psi_{t,t+1} + c\beta_p[a(W - P_t) + h(\psi_{t,t+1} - g)]. \end{cases} \tag{8}$$

The focus of our analysis will be to undertake a global analysis of the map (8), showing how, in the regions of the parameters space where the equilibrium point is unstable, a different attractor may exist having "good" properties from a practical point of view. That is, even if the fixed point of the economy is unstable, we can predict its "fate" in a macroscopic way giving, for example, the width of the oscillations that the state variables such as P_t can undergo.

3. General properties of the map

In this section we investigate the nature of the map driving the dynamics of the model as well as its regions of stability and invertibility/non-invertibility.

3.1. The map

From the previous section, the time evolution of price and chartists' expectations is obtained by the iteration of the two-dimensional non-linear map Q: $(\psi, P) \to (\psi', P')$

$$Q : \begin{cases} \psi' = (1 - c)\psi + c\beta_p[a(W - P) + h(\psi - g)] \\ P' = P + \beta_p[a(W - P) + h(\psi - g)], \end{cases} \tag{9}$$

[3] In order to remain mathematically tractable our model does not take into account the possible large positive or negative inventory positions of the market maker. Day and Huang suggest how these could be taken into account in the way the market maker adjusts the new price. We leave the analysis of such effects to future research.

where the symbol $'$ denotes the unit time advancement operator. The map Q has the point $(\overline{\psi}, \overline{P}) = (0, W + 1/ah(-g))$ as unique fixed point, so that in equilibrium fundamentalist demand is $-h(-g)$ (> 0) and chartist demand is $h(-g)(< 0)$, i.e. in equilibrium fundamentalists are net buyers (since the price is below their estimated long run mean) and chartists are net sellers. Of course, this situation cannot be considered a true equilibrium situation, it is a result of the fact that our dynamic model is in fact a partial one in that it leaves in the background the market for the alternative asset. A general analysis would need to take into account the dynamics of the alternative asset. Then $(\psi - g)$ would be replaced by a single quantity, φ say, which would be the chartists expectation of the difference in price change of both asset prices. We would then be dealing with a three-dimensional dynamical system, at whose steady state it turns out that $\varphi = 0$ and $\overline{P} = W$. Our analysis should thus be seen as that of a two-dimensional projection of this (more difficult to analyse) three-dimensional system. For more details of the full three-dimensional system and some preliminary analysis of its dynamics we refer the reader to Chiarella et al. (2001a).

By introducing the log price deviation $p = P - \overline{P}$ we obtain the new map $T : (\psi, p) \to (\psi', p')$ given by:

$$T : \begin{cases} \psi' = (1 - c)\psi - c\beta_{\mathrm{p}}[ap - k(\psi)] \\ p' = p - \beta_{\mathrm{p}}[ap - k(\psi)], \end{cases} \tag{10}$$

where $k(\psi) = h(\psi - g) - h(-g)$, and having the origin $\mathrm{O} = (0, 0)$ as unique fixed point.

3.2. Local stability conditions

The local stability of the fixed point O depends on the Jacobian matrix of the map[4] T,

$$DT(\psi, p) = \begin{bmatrix} 1 - c + c\beta_{\mathrm{p}} \dfrac{\gamma}{1 + (\psi - g)^2} & -ac\beta_{\mathrm{p}} \\ \beta_{\mathrm{p}} \dfrac{\gamma}{1 + (\psi - g)^2} & 1 - a\beta_{\mathrm{p}} \end{bmatrix},$$

at $(0, 0)$. Denote by Tr and Det the trace and the determinant of $\mathrm{DT}(0, 0)$, respectively, and by $\mathcal{P}(z) = z^2 - \mathrm{Tr}\, z + \mathrm{Det}$, the associated characteristic polynomial. A well known necessary and sufficient condition to have all the eigenvalues of $\mathcal{P}(z)$ less than 1 in absolute value (and thus a locally attracting fixed point) consists of the inequalities:[5]

$$\mathcal{P}(1) = 1 - \mathrm{Tr} + \mathrm{Det} > 0, \quad \mathcal{P}(-1) = 1 + \mathrm{Tr} + \mathrm{Det} > 0, \quad \mathcal{P}(0) = \mathrm{Det} < 1. \tag{11}$$

For our map the conditions (11) can be rewritten as:

$$\begin{cases} a\beta_{\mathrm{p}}(2 - c) < 2(2 - c) + 2c\beta_{\mathrm{p}}k'(0), \\ a\beta_{\mathrm{p}}(1 - c) > c[\beta_{\mathrm{p}}k'(0) - 1]. \end{cases} \tag{12}$$

Fig. 1 represents the region of local stability of the origin in the parameter plane (c, a), $0 < c \leq 1$, $a > 0$. From (12) it follows that, starting from parameters (c, a) inside the

[4] Note that for the assumed functional form of h, $k'(\psi) = \gamma/[1 + (\psi - g)^2]$.

[5] See, for instance, Gumowski and Mira (1980, p. 159).

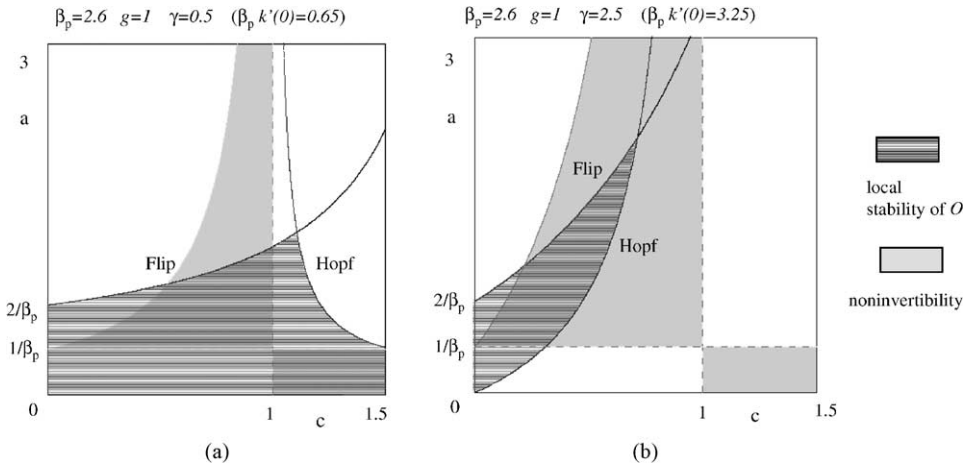

Fig. 1. The dark grey regions show the domain of stability of the equilibrium point O. The light grey regions represent the domain of non-invertibility of the map T. In (a), $\beta_p k'(0) \leq 1$ and in (b), $\beta_p k'(0) > 1$.

stability region, a loss of stability may occur either via a flip bifurcation, when crossing the curve

$$a = \frac{2}{\beta_p} + \frac{2ck'(0)}{2-c} \qquad \text{(Flip-curve)}, \tag{13}$$

or via a Neimark–Hopf bifurcation, when crossing the curve

$$a = \frac{c[\beta_p k'(0) - 1]}{\beta_p(1-c)} \qquad \text{(Hopf-curve)}. \tag{14}$$

By assuming $\beta_p > 0$ as fixed, we notice that the shape of the stability region in the parameter plane (c, a), indicated in dark grey in Fig. 1, is greatly affected by the strength of chartists' demand at the steady state ($k'(0)$).[6] In particular, when $\beta_p k'(0) \leq 1$ (Fig. 1a) the region appears wider than in the opposite case (Fig. 1b). Fig. 1a shows that, when strength of chartist demand is relatively weak ($k'(0) < 1/\beta_p$), at a given level of chartists reaction speed (c) the equilibrium is stable for sufficiently low values of the fundamentalists reaction parameter a, but fundamentalists can cause instability by reacting too strongly to the deviation from the fundamental value. Fig. 1, shows that when strength of chartist demand is relatively strong ($k'(0) > 1/\beta_p$), the ability of fundamentalists' demand to stabilise the system is restricted to a fairly narrow range of the parameter a.

3.3. Invertibility of the map

For particular values of the parameters, the map T is a non-invertible map of the plane. This means that, while starting from some initial values (say $(\psi_{0,1}, p_0)$) the forward iteration

[6] We recall that for the particular chartist demand function that we have chosen, we have $k'(0) = \gamma/(1+g^2)$.

of (10) uniquely defines the trajectory $(\psi_{t,t+1}, p_t) = T^t(\psi_{0,1}, p_0)$ $(t = 1, 2, \dots)$, the backward iteration of (10) is not uniquely defined. In fact, a point (ψ, p) of the plane may have several rank-1 preimages.[7]

Let us assume $h(\cdot) = \gamma \arctan(\cdot), \gamma > 0$, so that $k(\psi) = \gamma \arctan(\psi - g) - \gamma \arctan(-g)$. It can be shown by elementary geometrical arguments that, by defining

$$m = (a\beta_p - 1)\frac{(1-c)}{c}, \tag{15}$$

the map has a unique inverse for $m \leq 0$ or $m \geq \gamma\beta_p$, while for $0 < m < \gamma\beta_p$ the map is non-invertible. In particular, by defining

$$\psi_1 = g - \sqrt{\frac{\gamma\beta_p}{m} - 1}, \quad q_1 = \beta_p k(\psi_1) - m\psi_1, \tag{16}$$

$$\psi_2 = g + \sqrt{\frac{\gamma\beta_p}{m} - 1}, \quad q_2 = \beta_p k(\psi_2) - m\psi_2, \tag{17}$$

the points (ψ, p) of the phase plane for which the function

$$q(\psi, p) = a\beta_p p - \frac{a\beta_p - 1}{c}\psi, \tag{18}$$

satisfies $q(\psi, p) < q_1$ or $q(\psi, p) > q_2$ have a unique rank-1 preimage, while the points for which: $q_1 < q(\psi, p) < q_2$ have three distinct rank-1 preimages. Thus, following the notation used in Mira et al., for $0 < m < \gamma\beta_p$ this map is of the type $Z_1 - Z_3 - Z_1$, which means that the phase plane is subdivided into different regions Z_j $(j = 1, 3)$, each point of which has j distinct rank-1 preimages. Such regions are bounded by the so-called *critical curves* of rank-1, defined as the locus of points having at least two *merging* rank-1 preimages (see Gumowski and Mira). For our map this set is defined as

$$\mathrm{LC} = \{(\psi, p) \in \boldsymbol{R}^2 : q(\psi, p) = q_1 \cup q(\psi, p) = q_2\}, \tag{19}$$

where q_1 and q_2 are given in (16) and (17), respectively, and it is therefore made up of two straight lines, say $\mathrm{LC} = L \cup L'$, where L and L' have the equations

$$L : p = \frac{a\beta_p - 1}{a\beta_p c}\psi + \frac{q_1}{a\beta_p}; \qquad L' : p = \frac{a\beta_p - 1}{a\beta_p c}\psi + \frac{q_2}{a\beta_p}. \tag{20}$$

Each of the *critical points* $(\psi, p) \in \mathrm{LC}$ has two *merging* rank-1 preimages, and the locus of such preimages, denoted by LC_{-1} (this defines the *critical curve* of rank-0), turns out to be made up of two straight lines, say $\mathrm{LC}_{-1} = L_{-1} \cup L'_{-1}$, whose equations are

$$L_{-1} : \psi = g - \sqrt{\frac{\gamma\beta_p}{m} - 1}; \qquad L'_{-1} : \psi = g + \sqrt{\frac{\gamma\beta_p}{m} - 1}. \tag{21}$$

The critical curve LC_{-1} corresponds here to the locus of points (ψ, p) of the phase plane in which the determinant of the Jacobian matrix $DT(\psi, p)$ vanishes.[8] Also the images of the

[7] Given a n-dimensional map $F : \boldsymbol{R}^n \to \boldsymbol{R}^n$ and a positive integer r we say that the point $\boldsymbol{y}$ is a rank-r preimage of the point $\boldsymbol{x}$ if $F^r(\boldsymbol{y}) = \boldsymbol{x}$, i.e. if $\boldsymbol{y}$ is mapped into $\boldsymbol{x}$ in r iterations.

[8] Generally speaking, for a differentiable map the critical curve LC_{-1} is a subset of the locus of points of the phase plane for which the determinant of the Jacobian matrix of the map vanishes.

set LC are called *critical curves* of higher rank, in particular $\mathrm{LC}_k = T^k(\mathrm{LC}) = T^{k+1}(\mathrm{LC}_{-1})$ (for $k = 0, 1, 2, \ldots$) are called *critical curves of rank* $-(k+1)$ ($\mathrm{LC}_0 = \mathrm{LC}$). In our example these always have two branches so that $\mathrm{LC}_k = L_k \cup L'_k = T^{k+1}(L_{-1}) \cup T^{k+1}(L'_{-1})$.

In order to compare the bifurcation curves in the parameter plane (c, a) with the ranges of invertibility or non-invertibility of the map T, it is useful to draw on the same (c, a) plane the region in which the non-invertibility condition $0 < m < \gamma\beta_\mathrm{p}$ is fulfilled. Taking into account Eq. (15), the condition $m > 0$ can be rewritten as $0 < c < 1$, $a > 1/\beta_\mathrm{p}$, while the condition $m < \gamma\beta_\mathrm{p}$, becomes $0 < c < 1$, $a < \gamma c/(1-c) + 1/\beta_\mathrm{p}$. The non-invertibility region of the map T is indicated in light grey in Fig. 1. It is worth noting that the higher is the value of γ, i.e. the strength of chartist demand at the steady state $k'(0)$, the wider is the non-invertibility region. Moreover, we can see that in the region defined by $0 < c < 1$, $a < 1/\beta_\mathrm{p}$, the map is invertible no matter what the value of $k'(0)$.

In the next section we shall investigate the dynamics of the map in different regions of the parameters space, mainly in order to highlight the impact of the parameter c, measuring the speed of adjustment of chartists' expectations. We will focus, in particular, on the case $\beta_\mathrm{p}k'(0) > 1$ (i.e. strength of chartist demand is relatively strong) in which, as we can see from Fig. 1b, the equilibrium "soon" becomes unstable as the parameter c is increased.

4. The Neimark–Hopf bifurcation and related global bifurcations in attracting sets

This section describes some of the possible types of dynamical behaviour of the model (8) when the parameters are allowed to vary both within the stability region for the equilibrium point O and beyond that region where the Neimark–Hopf curve is crossed. As already remarked in Section 3, assuming the parameter $c \in (0, 1)$, we have to consider two cases, qualitatively represented in Fig. 1. That is, if $\beta_\mathrm{p}k'(0) < 1$ (i.e. chartist demand is relatively weak), then we have a wide stability region (Fig. 1a) which includes any value $c \in (0, 1)$ for sufficiently low values of the parameter a, and stability is lost only via a Flip bifurcation as the strength of fundamentalist demand a is increased. When $\beta_\mathrm{p}k'(0) > 1$ (i.e. chartist demand is relatively strong) the stability region is reduced (Fig. 1b) and at low values of a, the fixed point undergoes a Neimark–Hopf bifurcation, while the Flip-curve still exists for high values of a. We have observed numerically that the crossing of the Flip curve very often results in an increase in the basin of divergent paths, which is economically not an interesting case. Hence, this section considers only examples of the Neimark–Hopf bifurcation.[9]

4.1. Stability region

Let us assume $\beta_\mathrm{p} = 2.6$, $g = 1$ and $\gamma = 2.5$ so that $\beta_\mathrm{p}k'(0) = 3.25 > 1$, and consider a point belonging to the stability region. Fig. 2a shows a trajectory in the phase-plane which spirals around the attracting focus O. In this example the basin of attraction of O, say $\mathcal{B}(\mathrm{O})$, which is the locus of points whose trajectories converge to the stable equilibrium, is a fairly wide region of the phase-plane. However, it is worth noting that for different values of the parameters c and a, always inside the stability region represented in Fig. 1b, we observe via

[9] We refer the reader to Chiarella et al. (2001) for a more detailed analysis of the Flip bifurcations.

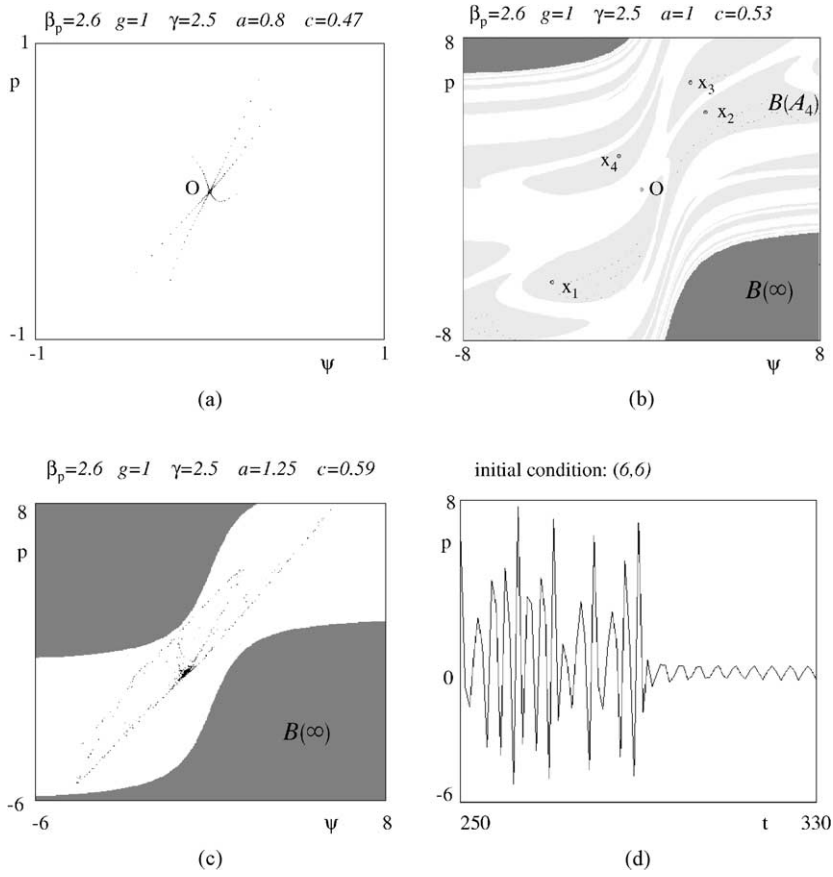

Fig. 2. Different dynamic phenomena observed when the equilibrium point O is stable.

the examples in this section several other dynamic phenomena besides the attracting fixed point O. In particular, we may also have (i) a coexisting attractor (regular or chaotic), (ii) points having divergent trajectories, and (iii) a chaotic repellor.

In case (i), we denote by $\mathcal{A}$ the coexisting attractor, and by $\mathcal{B}(\mathcal{A})$ its basin of attraction which, as we shall see, may also be wider than $\mathcal{B}(\mathrm{O})$. Case (ii) is quite common in non-linear maps, but we are interested to see if such points are close to or far away from the attractors. Such points, which are not meaningful in a practical sense since they imply exploding prices and returns, may be viewed as points converging to an attractor at infinity, on the "Poincaré equator", i.e. an improper point of the phase-plane. We shall denote by $\mathcal{B}(\infty)$ the set of points having divergent trajectories (basin of attraction of a point at infinity). The complementary set in the phase-plane is the set of points having bounded trajectories. As noticed in case (i) above, this set may be shared between two or more co-existing attracting sets.

An example is given in Fig. 2b where besides the stable focus O there exists a coexisting attracting four-cycle $\{x_1, x_2, x_3, x_4\}$ labelled $\mathcal{A}_4$. The white region denotes the closure of

the basin $\mathcal{B}(O)$ while the closure of the basin $\mathcal{B}(\mathcal{A}_4)$ is in light grey. A third attractor is at infinity, and the basin $\mathcal{B}(\infty)$ is the dark grey region. It is thus clear from this figure that, although the unique fixed point of the system may be locally stable, we must be cautious in asserting that the economy approaches the (locally) attracting equilibrium, because the time evolution depends strongly on the initial state.

The diagrams in Fig. 2 indicate the importance of the "robustness" of the stability property with respect to external shocks, which may abruptly move the state of the system into a different basin of attraction. For example we can certainly say that the stability of the fixed point O in Fig. 2a is robust with respect to external perturbations. From any initial condition in that region, trajectories converge towards the stable focus, a shock simply moves the point in the phase-plane to another initial condition in the same basin. The effect of the shock is simply a slight quantitative change in the oscillatory converging motion to the fixed point. This is no longer true in the case shown in Fig. 2b. In fact, even if we start from an initial condition in $\mathcal{B}(O)$, a shock may push the phase-point into a different basin of attraction, thus, changing the qualitative behaviour of the trajectory. Trajectories may ultimately converge to the attracting cycle $\mathcal{A}_4$ or even diverge.

It is important to note that in the case of a non-invertible map, as is the case in this regime, the basins of attraction of coexisting attracting sets are generally not connected (a property which cannot occur in invertible maps). It is evident that the basin (in light grey) of the four-cycle $\mathcal{A}_4$ in Fig. 2b is not connected. The basins have such a structure because the total basin is obtained by taking all the preimages of any rank of the "immediate basin". Precisely, the immediate basin of $\mathcal{A}_4$ is obtained by considering the four fixed points of the map T^4. For each point, we take the widest simply connected area included in the basin that contains it. The immediate basin $\mathcal{B}_I$ of the four-cycle of T is the union of four disjoint, cyclical areas.[10] Then the whole basin is $\mathcal{B}(\mathcal{A}_4) = \cup_{n\geq 0} T^{-n}(\mathcal{B}_I)$, and we obtain the light grey area shown in Fig. 2b.

The complementary set of $\mathcal{B}(\infty)$ may also display a different structure. Instead of coexisting attractors (which may also be the stable fixed point O and a chaotic attractor), we may have coexistence of the stable fixed point with a strange repellor, as already remarked in (iii). The presence of such an "invisible chaos" shows up in the transient part of the trajectory.[11] An example is shown in Fig. 2c. There the grey region denotes $\mathcal{B}(\infty)$ while the white region gives the closure of the basin $\mathcal{B}(O)$. This means that any point in the white region, except for a set Λ of zero Lebesgue measure, has a trajectory converging to O. Fig. 2d shows the strange behaviour in the transient part of the trajectory that can occur in this situation. It is clear that if we restrict our interest to a "short period", as is often the case in applications, then it is difficult to "classify" the robustness of the stability of O.[12]

[10] That is the four light grey areas in Fig. 2b containing the points x_1, x_2, x_3 and x_4.

[11] The formation of such a chaotic repellor is often due to a sequence of flip bifurcations of saddles, changing the saddles into *repelling nodes* and giving rise to *saddle cycles of double period*.

[12] In the case of Fig. 2c and d the dynamic behaviour over a short time is the same as the one observed when O is unstable and a chaotic attractor exists around it (as we shall see again later). Thus, looking at the transient part we cannot predict if the system is stable or unstable, i.e. whether the state will ultimately settle on the stable fixed point or if it will wander chaotically, and unpredictably, around it.

4.2. Crossing the Neimark–Hopf bifurcation curve

Now we consider the types of dynamic behaviour that may occur when the fixed point becomes unstable via a crossing of the Neimark–Hopf bifurcation curve. Starting from inside the stability region of Fig. 1b with a value of a sufficiently high, an increase of the parameter c leads to oscillatory behaviour which may become chaotic around O, and as c approaches the value 1 the dominating state is an attracting cycle (although coexisting with a strange repellor) with a wide basin of attraction. While when the same Hopf-curve is crossed at low values of the parameter a, we have numerically observed a stronger "stability effect", with persistence of regular oscillations.

Let us fix $a = 0.8$ and increase the parameter c. When crossing the Neimark–Hopf bifurcation curve we observe a supercritical bifurcation, leaving a repelling focus O surrounded by the attracting closed invariant curve Γ in Fig. 3a, on which the trajectories are either periodic (when the *rotation number* at the Neimark–Hopf bifurcation is rational) or quasi-periodic (when the rotation number is irrational), as described in Mira (1987).

In Section 5 we shall see the effects of the non-invertibility of the map, which shall lead us to the construction of an *absorbing area* inside which the attractors are confined. Here we simply observe that local and global bifurcations occurring to the attracting set existing around O give rise to a chaotic attractor $\mathcal{A}$ of "annular shape", as the one shown in Fig. 3b. Such a chaotic attractor $\mathcal{A}$ is generally the final effect of a period-doubling route, set off by the appearance of a stable cycle on the closed invariant curve Γ. The behaviour of the trajectory in such a case is a kind of "permanent" erratic transient. The phase point wanders inside a chaotic area in an unpredictable way. However, as we shall show in Section 5, in the non-invertible case the structure of the phase-plane in zones with a different number of rank-1 preimages (also called *Riemann foliation*[13] in Mira et al.), enables us to predict the strip inside which the state variables are confined. That is, even if, given a state, we cannot predict what will be the state in the next period, we can determine its lower and upper bound, which means that we can relate the volatility of returns to the parameters of the model.

As c increases, several regimes with "periodic windows" and "chaotic areas" may be observed. This regime is a two-dimensional analogue of what occurs in one-dimensional chaotic maps. On further increasing c (at values of the parameter a not too high), we observe the appearance of a periodic regime, which persists as c approaches the value 1. An example of an attracting cycle appearing after the chaotic regime is given in Fig. 3c . We note that in this case a strange repellor Λ surrounding the stable cycle is likely to exist, and it is possible that looking at the trajectories over a "short period" there is not much difference between the case of Fig. 3b and that of Fig. 3c. The difference is evident over a longer period or when the initial state is quite close to a periodic point of the cycle. In all the three situations shown in Fig. 3, we may consider the existing attractor (a closed curve Γ, a chaotic area $\mathcal{A}$ or a stable cycle) as "robust" with respect to external influences. In fact, the basin $\mathcal{B}(\infty)$ is quite

[13] As described in Mira et al., in the case of two-dimensional non-invertible maps the phase-plane can be identified with several "sheets", each being associated with one inverse of the map. The non-invertibility is thus characterized by the *overlapping* of different sheets constituting the regions Z_j (with j different rank-1 preimages) and the boundaries of these regions are generally given by the critical curves of rank-1, crossing which the number of distinct rank-1 preimages changes. This characterization is known as the *foliation* of the Riemann phase-plane.

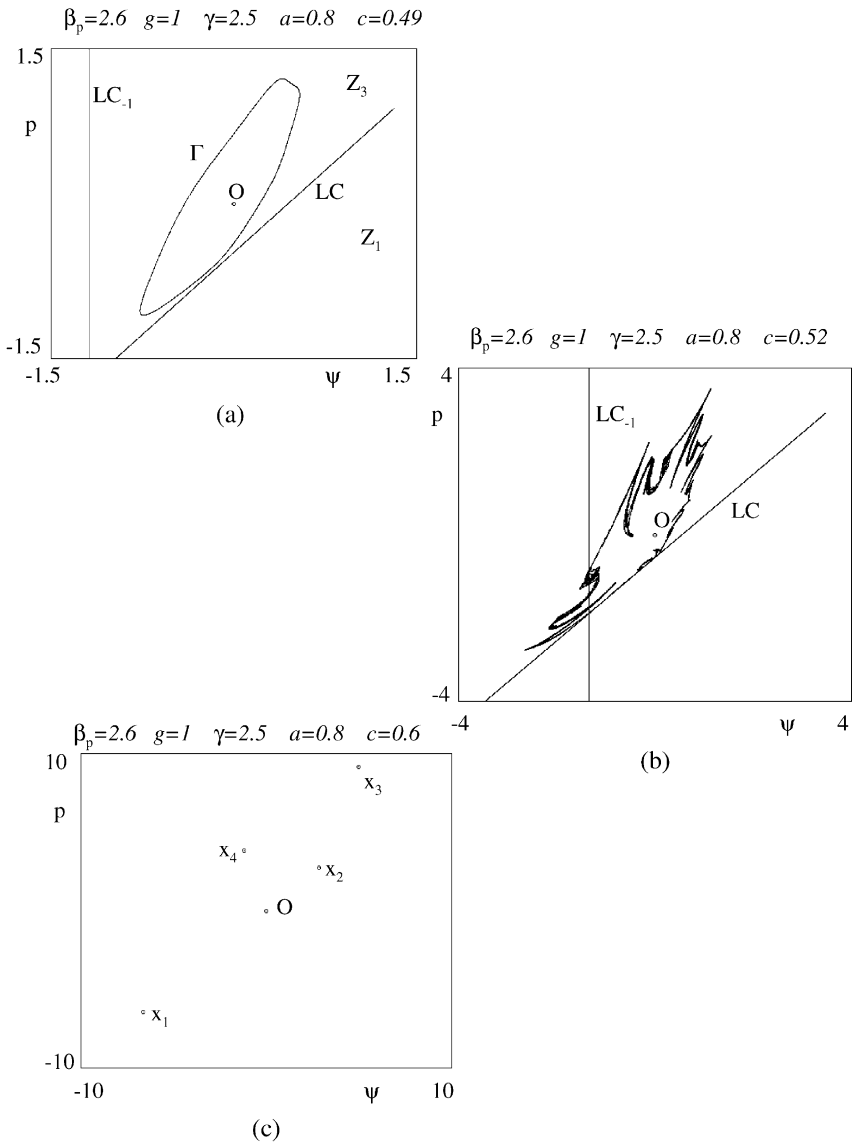

Fig. 3. Dynamic behaviour observed by increasing c starting from outside the stability region of O, on the right of the Neimark–Hopf bifurcation curve in Fig. 1b.

far from such attracting sets and almost all the points in the region of the phase-plane shown in the figures have a similar qualitative behaviour. This kind of "robustness" is increased at lower values of a.

When crossing the Hopf-curve at low values of a, an attracting closed curve Γ is observed, but no route to chaotic regimes: we have numerically observed that the oscillatory behaviour

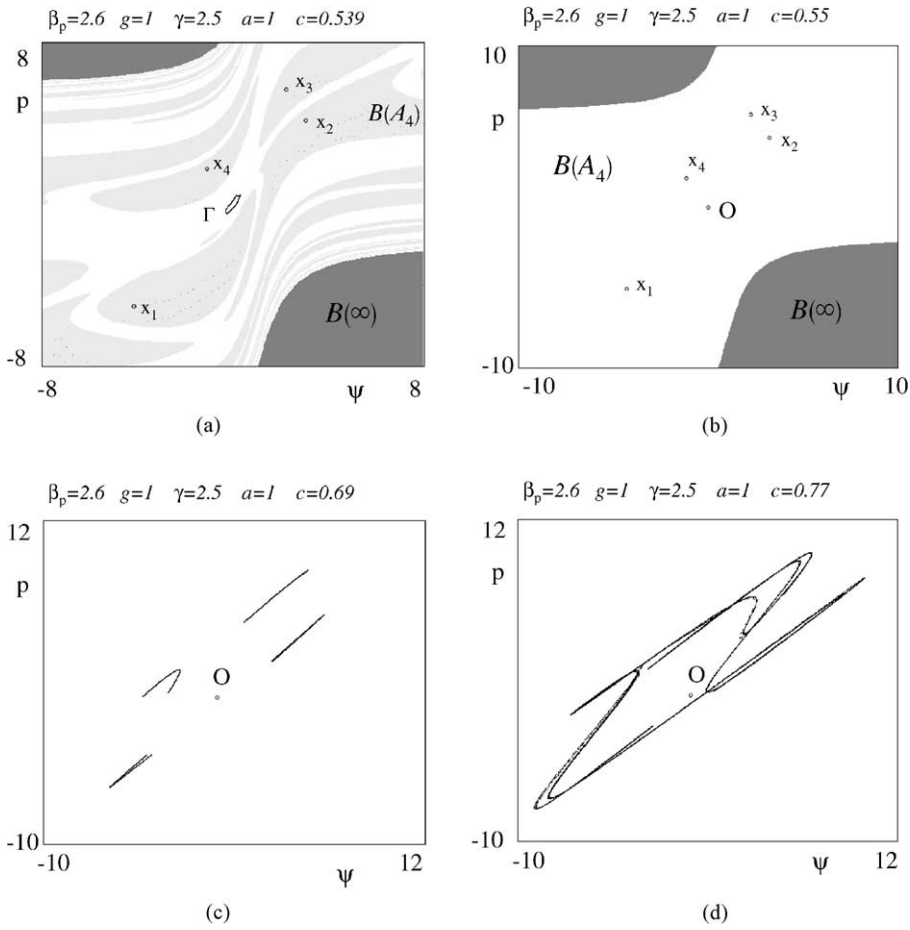

Fig. 4. Increasing c with respect to the situation represented in Fig. 2b.

persists and the oscillations become wider as a is decreased. Whereas, on increasing a the system goes towards a less stable regime, as already remarked in the previous section. For example, at $a = 1$ we have already seen the stable fixed point coexisting with an attracting four-cycle in Fig. 2b. On increasing c from that situation we cross the Hopf-curve and an attracting closed invariant curve Γ appears. However we already know from Fig. 2b that O is not far from the boundary of its basin, and the same is true for Γ, as shown in Fig. 4a. This leads us to foresee that the interval of values of c for which an attracting closed invariant curve exists will be very short. In fact, a global bifurcation occurs when the attracting set has a contact with the frontier of its basin of attraction. In our example this contact occurs in a point belonging to the frontier between the basin of Γ and the basin of the four-cycle $\mathcal{A}_4$. Thus, after the contact, the only surviving attractor is the four-cycle $\mathcal{A}_4$, as shown in Fig. 4b. We note that this contact bifurcation also corresponds to a global bifurcation of the basin $\mathcal{B}(\mathcal{A}_4)$, which increases abruptly. The closure of $\mathcal{B}(\mathcal{A}_4)$ is now the white region in

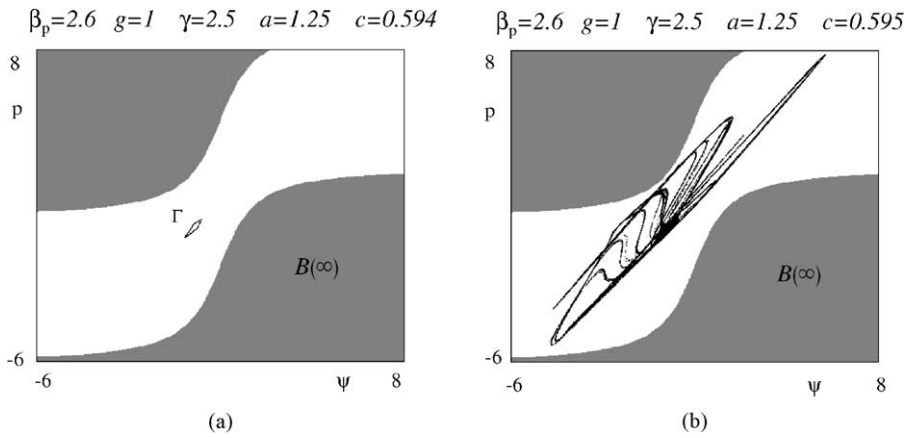

Fig. 5. The same parameter values as in Fig. 2c, but with a value of c slightly increased.

Fig. 4b and this new attracting set is also stable with respect to perturbations, being quite far from the boundary of its basin. We also note that only a few unstable cycles exist in that white region. From this cycle of period 4 the usual route to chaos via period doubling bifurcations is observed as c is further increased. A four-piece chaotic attractor is shown in Fig. 4c and a global bifurcation leads to the reunion of the chaotic pieces into a single attractor of annular shape, shown in Fig. 4d.

Similarly, when we start from the situation shown in Fig. 2c and increase c we observe, on crossing the Hopf-curve, an attracting closed invariant curve Γ. Also now we shall have a global bifurcation causing the destruction of Γ, but differently from the previous case: it cannot be predicted by the position of Γ with respect to $\partial\mathcal{B}(\infty)$. In fact, as shown in Fig. 5a, Γ is quite far from that boundary. But it is the existence of the strange repellor Λ that will cause the global bifurcation. A contact between Γ and the strange repellor causes a homoclinic explosion (or Γ-explosion) which transforms the strange repellor into a strange attractor, as shown in Fig. 5b, after a very small increase of c. Such a global bifurcation has a very strong effect on the "observed attractor", because after the disappearance of the attracting set around O the generic trajectory wanders, aperiodically, within the chaotic set (which was previously "invisible", except for the transient part of a trajectory).

5. Role of the critical curves in the global bifurcations

This section discusses in more detail the mechanism underlying some of the global bifurcations, by showing how the non-invertibility of the map for the examples of Section 4 (which at first sight seems to lead to an increase of difficulty) allows us to easily explain important bifurcation phenomena. We again use the powerful technical tool of the *critical curves*, first using them to construct an absorbing area, i.e. an area bounded by a few arcs of critical curves LC, $LC_1, \ldots$, which attracts nearby points and is trapping (once inside, a trajectory can never escape). Clearly, inside one absorbing area we have at least one

attracting set; moreover, inside an absorbing area several attractors may follow one another, and the area itself may undergo global bifurcations.

The critical curves represent the two-dimensional analogue of the critical points (local extrema) in the dynamics of one-dimensional non-invertible maps (see *kneading theory* in Devaney (1987) and Collet and Eckmann (1980)). Just as it occurs for the local extrema in one-dimensional maps, the critical curves bound the foliation of the Riemann phase-plane. Knowledge of the critical curves and of the absorbing areas gives us a quick and easy method to determine whether a repelling node or focus is a *snap-back-repellor*, as described below. Moreover, as stated in Section 4.2, a knowledge of the absorbing areas is important as it allows us to understand the basic determinants of the volatility of returns in our model.

5.1. Absorbing areas

Consider again the case shown in Fig. 3a. As the parameter c is increased the closed invariant curve Γ increases in size, and the non-invertibility of T comes to play a role as Γ approaches and then crosses the critical curve LC_{-1}. Note that from Fig. 3a it seems that Γ is closer to LC than to LC_{-1} and that a contact with LC might come first. But this is impossible given the structure of the Riemann foliation of the zones Z_1–Z_3 bounded by LC. To make a one-dimensional analogue, consider an interval J mapped by the *logistic map* $f(x) = \mu x(1 - x)$. Clearly $f(J)$ cannot cross the local maximum, denoted by C; $f(J)$ can only have C on the boundary and this can occur only if J includes the critical point C_{-1}. In the same way the critical curve LC cannot be crossed, the arcs crossing LC_{-1} are mapped by T into arcs "folded" on LC and tangent to that curve.

Consider Fig. 6a. The crossing of LC_{-1} causes the appearance of "oscillations" in the smooth shape of Γ, due to the "folding" on LC and its further images. In fact, the portion of Γ which crosses LC_{-1} (in the points a_0 and b_0) is folded back with two points of tangency on LC (see a_1 and b_1 in Fig. 6a, where also the points a_2 and b_2 of tangency on LC_1 are indicated as well as the points of tangency on critical curves of higher rank). More crossings of LC_{-1} as c increases may occur, which are the cause of more oscillations in the shape of Γ, as shown in Fig. 6b. We remark that such qualitative changes in the shape of Γ modify the quasi-periodic orbit of the asymptotic trajectories. Moreover, we can completely define the area enclosing Γ by means of the critical curves. In fact, making use of the techniques described in Chapter 4 of Mira et al., we take a suitable piece of LC_{-1}, and with a few iterates of this segment we obtain a closed area, simply connected, which is mapped into itself by T (see again Fig. 6a and b); Γ is tangent to the boundary of this area in several points (those on LC and their images). Moreover, with a few more iterates of the same arc on LC_{-1}, an "inner" boundary is also obtained. Thus an absorbing area of annular shape is soon defined (Fig. 6b), to both of whose external and internal boundaries Γ is tangent (see the enlargement in Fig. 6c).

As c is further increased, several attracting sets alternate inside the absorbing area: quasi-periodic orbits, periodic orbits, flip sequences leading to chaotic dynamics, as was shown in Fig. 3 in the previous section. The annular attracting set of Fig. 3b is inside an annular absorbing area. Another example is given in Fig. 7a. A small portion of LC_{-1} in that figure was iterated 19 times and the resulting set is an invariant absorbing area A_1, inside which the trajectories are confined. An orbit is shown in Fig. 7b. The critical curves

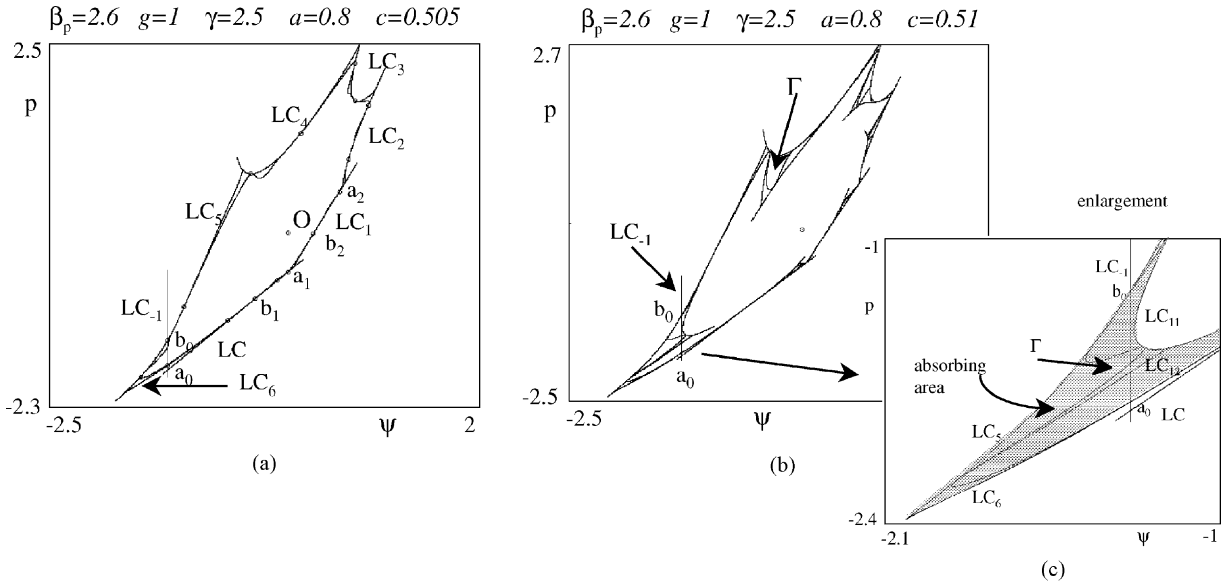

Fig. 6. Increasing c starting from outside the stability region of O, on the right of the Neimark–Hopf bifurcation curve in Fig. 1b.

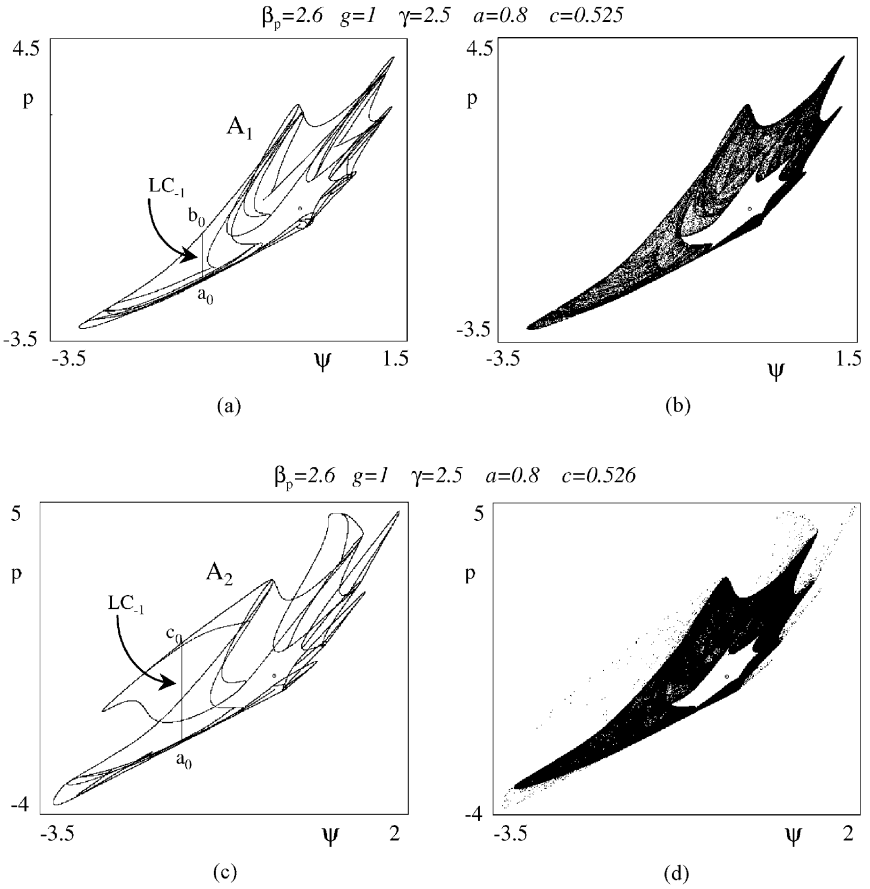

Fig. 7. An invariant absorbing area of annular shape, obtained by means of the critical curves.

allow us to predict the lower and upper bounds of both state variables, such limiting values being obtained from the rectangle bounding the absorbing area.

Considering the iterated points of a trajectory we find that a global bifurcation occurs at a particular value of c, say c^* (in our example $0.525 < c^* < 0.526$). For $c < c^*$, the iterated sequences are all inside the annular absorbing area as in Fig. 7a and b, whilst immediately, for $c > c^*$, some iterated points also go outside, although such "bursts" are quite rare, as shown in Fig. 7d. This is the effect of a global bifurcation due to the contact of the critical curves on the boundary of the absorbing area A_1 with a chaotic repellor existing outside. Such a contact destroys the invariance property of the area A_1 and after the bifurcation the iterated points can escape the old area A_1. These bursts could be a source of outliers of returns.

The bifurcation just refered to can be detected also by the use of critical curves. In fact, for $c < c^*$ the iterations of the small segment a_0b_0 of LC_{-1} define an area A_1 which is invariant, so that all the iterates $T^n(a_0b_0)$, $n > 0$, belong to that area. Whilst for $c > c^*$ the

area obtained by iterating the segment a_0b_0 of LC_{-1} is no longer invariant, i.e. there exists a positive integer m such that $T^m(a_0b_0)$ has points also outside. This corresponds to an "explosion" of the attracting set. After the contact the new iterates will cover a wider area, which we can predict by looking at the images of the critical segments. A wider portion of LC_{-1}, see a_0c_0 in Fig. 7c, is such that with a finite number of iterates we obtain a new wider absorbing area A_2 (which includes the old area A_1, no longer invariant). The boundary of the new absorbing area is strictly included in $\cup_{n=1}^{12} T^n(a_0c_0)$. From Fig. 7d, it is evident that A_2 is the smallest invariant absorbing area existing after the contact bifurcation that destroys A_1.

It is now clear that also the sequences of bifurcations shown in Figs. 4 and 5 of the previous section all occur inside similar absorbing areas. Regular and chaotic dynamics alternate inside an annular area around the repelling fixed point O.

5.2. *The homoclinic bifurcation of a snap-back repellor*

Consider again the annular absorbing area A_2 shown in Fig. 7. We see that a hole H exists including the fixed point O, a repelling focus. As locally the orbits spiral out from O, it turns out that all the points of $H\backslash\{O\}$ have orbits entering the trapping annular absorbing area. Thus, in such a situation, although the fixed point O is repelling, we cannot find any homoclinic orbit of the origin. The existence of a homoclinic orbit of a repelling focus O often causes the appearance of a set which "attracts" and then "repels" (as occurs in the case of homoclinic orbits to saddles). A trajectory behaves chaotically far from O, then it approaches and seems attracted to O, but soon after it is repelled away. This occurs with intermittency, and with unpredictable return time near O. The existence of such homoclinic orbits is a powerful tool used to prove the true chaotic nature of the observed orbits. In fact, Marotto (1978) first proved that such an orbit for a repelling node or focus implies the existence of chaos in the sense of Li and Yorke (1975).

In our example, the fixed point O is a repelling focus for a wide interval of values of c, i.e. for $c > \overline{c} \simeq 0.48$. However when is it possible to find some homoclinic orbits of O? Certainly we cannot look for homoclinic orbits as long as the map has a unique inverse, because in invertible maps, homoclinic orbits of repelling nodes and foci cannot exist: but in our example, when $a = 0.8$, the map T is non-invertible in the entire range of c for which O is unstable. In the regime of non-invertibility of T we can make use of the properties of the critical curves of the map (see Gardini, 1994) to find the homoclinic orbits of cycles. For example, although chaotic dynamics certainly exist for the map in the cases shown in Fig. 7, these do not involve the fixed point O. In fact, as long as the repelling fixed point belongs to an absorbing area, bounded by critical curves, but with a hole H surrounding O, then we can prove that all the preimages of any rank of O (which are infinitely many) are outside the absorbing area (and thus outside the chaotic area). This is true for all the points belonging to the hole H defined by the annular absorbing area, and it is an immediate consequence of the fact that the absorbing area is trapping. We note that other qualitative changes occur in the absorbing area, with tongues approaching O, but as long as the rank-1 preimages of O are outside the invariant absorbing area, then the critical curves leave an empty hole around O (see Fig. 8a and the enlargement in Fig. 8b), and no homoclinic points of O can exist. This is because for any $n > 0$, $T^{-n}(O)$ can never return near O.

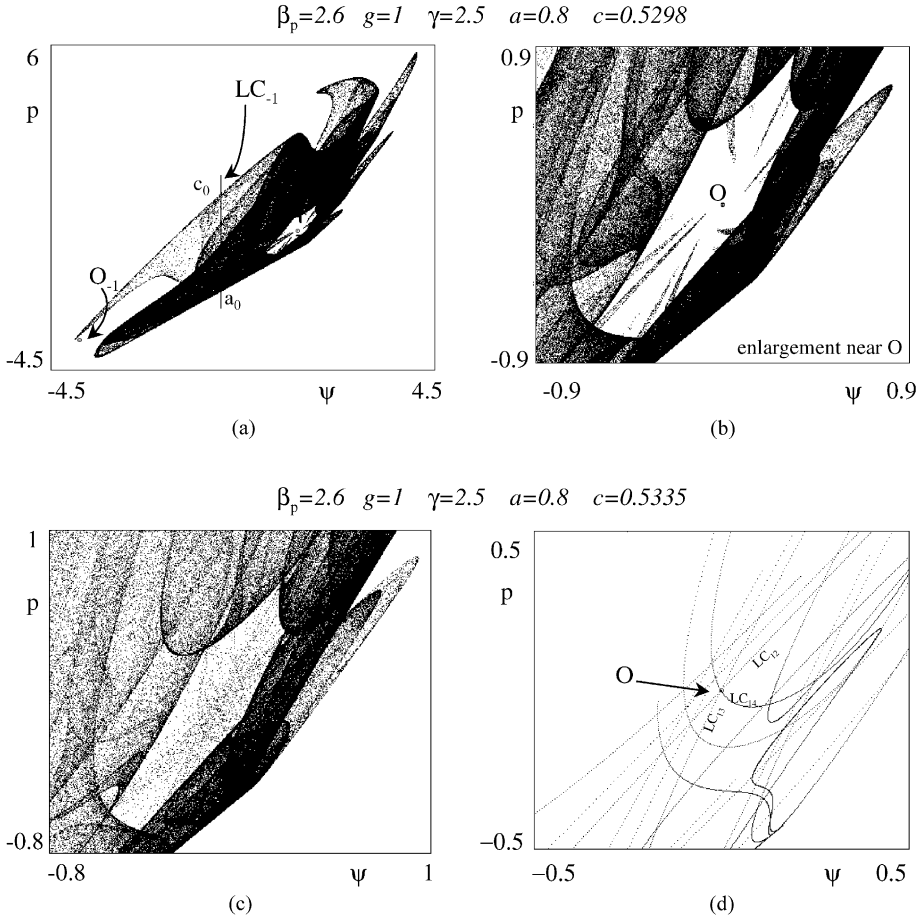

Fig. 8. The same parameter values as in Fig. 7 and $c = 0.5298$, a chaotic attractor, enclosed into an annular absorbing area, bounded by critical curves.

Then we can easily conclude that as c increases, the first homoclinic bifurcation, or homoclinic explosion, necessarily occurs when one of the rank-1 preimages of the fixed point O, from the outside of the absorbing area A_2, falls on the boundary and crosses it, through an LC arc. This occurs approximately at $c \simeq 0.5335$, at this value the hole surrounding O disappears (Fig. 8c). Even without computing the rank-1 preimages of O, we can be sure that we are at the homoclinic bifurcation of the fixed point, because at this particular value the images of the critical curves of LC must cross through O. As shown in the enlargement of Fig. 8d, all the images $LC_{12}, LC_{13}, LC_{14}, \ldots$ (LC_k for $k \geq 12$) of the LC curve cross the fixed point O, which means that one of its rank-1 preimages (say O_{-1}) lies now on the boundary of the absorbing area, on the curve LC_{11}. At this bifurcation value homoclinic orbits of O (and infinitely many) appear. In fact, the point O_{-1} on the curve LC_{11} of the boundary of the absorbing area must have a rank-1 preimage on the curve LC_{10},

and so on iteratively, up to a preimage in the segment of LC_{-1} inside the area A. In its turn, this point has an arborescent sequence of preimages of any rank inside the absorbing area A, and infinitely many of these preimages can be obtained with the local inverse near the fixed point O, thus giving *critical homoclinic orbits*. In fact, when c is at the first homoclinic bifurcation value, the characteristic property (see also Gardini) is that all the homoclinic orbits of O are critical (i.e. include a critical point). While soon after the bifurcation value infinitely many non-critical homoclinic orbits of O exist.

We have demonstrated above the true chaotic nature of the orbits observed in this particular regime of parameters. However, we have also found other regimes which seem chaotic (for instance with lower values of c). In order to prove that these regime are truly chaotic, it is sufficient to notice that the same properties discussed above for the fixed point could hold for a periodic orbit of any order: in other words, since the periodic points of a k-cycle, $k = 1, 2, \ldots$, are fixed points for the map T^k, all we have to do is to look for the existence of homoclinic orbits of these periodic points, by considering their preimages.

6. Some stochastic simulations

In Sections 4 and 5, we have analysed the global dynamic behaviour of our simple deterministic model of fundamentalists and chartists. The main dynamic behaviours that we have uncovered include various bifurcations, "invisible" chaos, disconnected basins of attraction and intermittent "bursts" out of and then back into attracting regions.

Any model aiming to capture the basic aspects of financial market dynamics also needs to take into account, along with heterogeneity of agents beliefs, the effect of stochastic factors. The important issue is to determine how the deterministic non-linear dynamic phenomena arising due to heterogeneous agents interact with the stochastic factors. Is it possible that some of the basic characteristics of time series of returns in financial markets such as volatility clustering, fat tails, peaked distributions and skewness have as their origin the interaction of the non-linear deterministic phenomena with the external noise impinging on the financial market?

Standard finance theory, implicitly, leaves no role for deterministic dynamic factors in explaining such behaviours. The standard dynamic models have stable deterministic parts (usually with monotonic trajectories) that are shocked by external noise factors, usually modelled as increments of Wiener processes, which are normally distributed. The task of reconciling the non-normally distributed returns that are the output of a stable dynamic system shocked by normally distributed noise is thrown onto the standard deviation (volatility) which is assumed to be some (unmotivated) function of the state variables and/or of the noise process itself (so-called heteroscedasticity, ARCH-effects etc.).

Models of the type developed in this paper leave a major role to the non-linear phenomena arising from the dynamic interaction of heterogeneous agents in explaining the types of return distributions displayed by financial market assets.

Stochastic factors could be considered either in the difference equation for p or in the difference equation for ψ or indeed in both. In the simulations reported here we have considered a stochastic factor in the difference equation for ψ. This captures, albeit in a crude fashion, the notion that the chartists adjust either aggressively or cautiously their

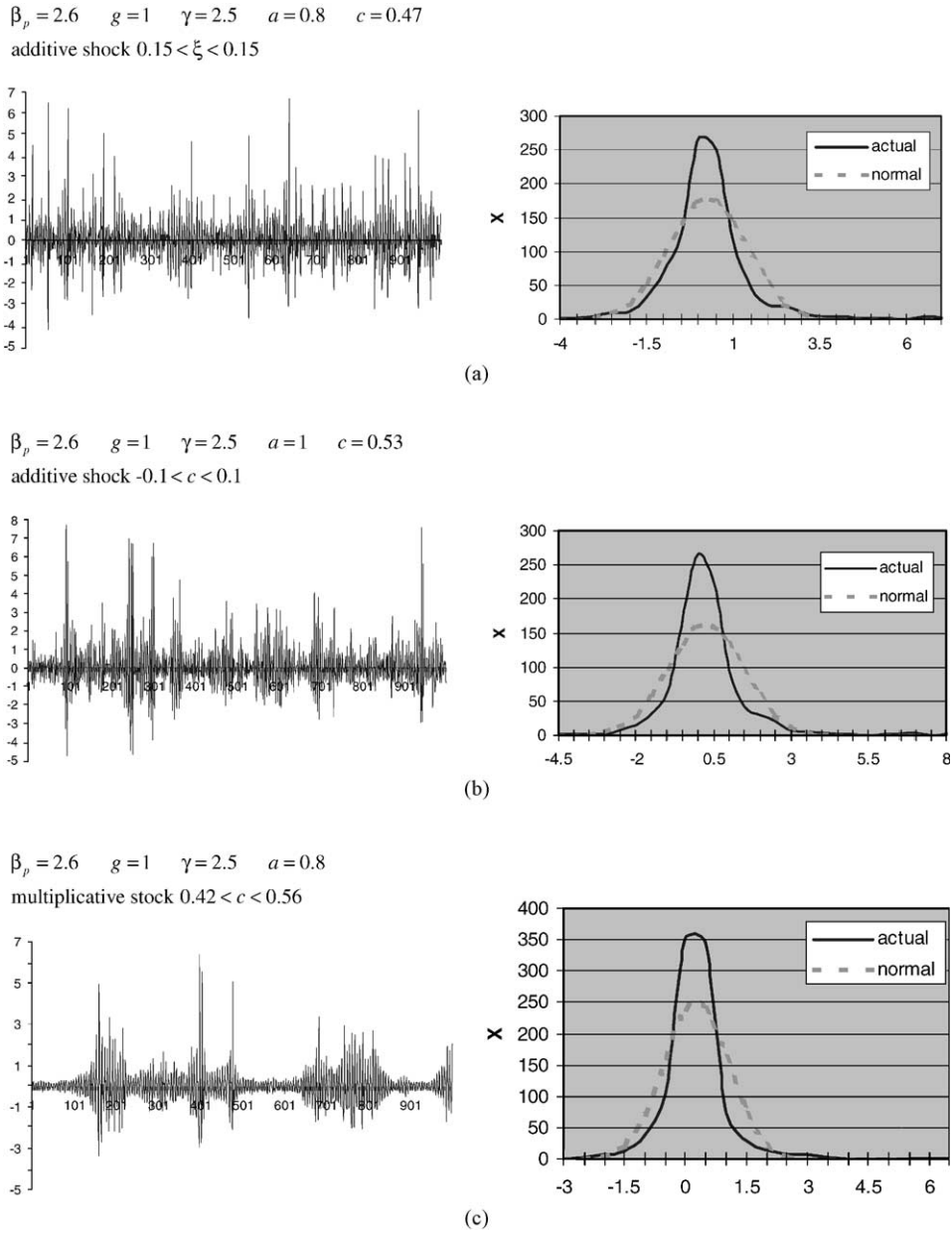

Fig. 9. Time series of returns and return distributions resulting from simulations of stochastic versions of the model.

estimate of expected return depending on whether there is a positive (good news) or negative (bad news) shock. We have considered two types of stochastic factors. The first additive, so that the map (10) would be written

$$\psi' = (1-c)\psi - c\beta_{\mathrm{p}}[ap - k(\psi)] + \xi_t, \qquad p' = p - \beta_{\mathrm{p}}[ap - k(\psi)], \tag{22}$$

where ξ_t is uniformly distributed on the interval $[\xi_{\min}, \xi_{\max}]$. The second multiplicative, in which the chartists' speed of adjustment of expectations varies randomly around some mean value. In this case the map (10) would be written

$$\boldsymbol{X}_{t+1} = T_{c_t}(\boldsymbol{X}_t), \tag{23}$$

where c_t is a random parameter uniformly distributed on the interval $[c_{\min}, c_{\max}]$ and T_{c_t} is the map given in (10) with the parameter c_t.

Fig. 9a displays the returns and the return distribution (compared with the corresponding normal distribution) resulting from a simulation of (22) with ξ_t distributed uniformly on $[-0.15, 0.15]$. The parameters of the model are those relevant to Fig. 2a. In this case the equilibrium is stable but with orbits converging to it in a cyclical fashion. The stochastic version of the model clearly shows both volatility clustering, fat tails, peaked distribution and skewness. Here, these are due solely to the oscillatory transients of the underlying deterministic model. In a sense this case is the closest to the vision of the stable deterministic part of the models of the standard finance paradigm, with the only additional feature being the oscillatory approach to the equilibrium.

Fig. 9b displays the returns and the return distribution resulting from a simulation of (22) with ξ_t distributed uniformly on $[-0.1, 0.1]$ and the parameters of the model are those relevant to Fig. 2b. Here also we see volatility clustering and the distributional characteristics of real financial data. These are most likely due to the fact that the noise is pushing the state variables between the (white) basin of attraction of the equilibrium and the (light grey) basin of attraction of the four-cycle.

Fig. 9c displays the returns and return distribution resulting from a simulation of (23) with c uniformly distributed on $[0.42, 0.56]$. The parameters of the model are those (apart from c) relevant to Fig. 3a and b. Thus, the variation of c causes the map to vary across a wide range of outcomes including a closed curve similar to Fig. 3a and a chaotic attractor similar to Fig. 3b. It is this variation across maps which is the origin of the volatility clustering and fat tails that we see in Fig. 9c.

The simulations of this section are very preliminary and have been chosen to illustrate qualitatively how the interaction of some of the non-linear deterministic phenomena of the model with a simple external noise source can give rise to the qualitative types of return behaviour observed in financial markets. We leave to future research the task of calibrating such models to actual market data and doing more extensive simulation studies.

7. Conclusions

In this paper we have developed a discrete time model of asset price dynamics, based on the interaction of two types of traders: fundamentalists, who hold an estimate of the fundamental value of the asset and whose demand is an increasing function of the difference

between the fundamental value and the current price, and chartists, a group basing its trading decisions on an analysis of past price trends, whose demand is an S-shaped function of the expected return differential with an alternative asset. We assume the existence of a *market maker*, whose role is to set excess demand to zero at the end of each trading period by taking an off-setting long or short position, and who announces the next period price as a function of the excess demand. We have demonstrated how the behaviour of the two types of traders affects the dynamics by showing the effect, on the local and global dynamics, of the key parameters, namely the "strength" of fundamentalist and chartist demand (a and γ, respectively), and the speed of adjustment of chartists' expectations (c). In particular we have clarified how the strength of chartist demand γ affects the local stability of the equilibrium, by showing that for sufficiently low values of γ the equilibrium is stable for a wide range of values of the fundamentalist parameter a and for any level of the chartists' reaction speed c ($0 < c \leq 1$); while when γ is sufficiently high, i.e. chartist demand is relatively strong, the ability of fundamentalists' demand to stabilise the system is restricted to a fairly narrow range of the parameter a. Our analysis then focused on the global dynamical behaviour observed in this latter case. First we have shown that also when the equilibrium is locally stable other dynamic phenomena arise for sufficiently high values of c and a, such as chaotic transients before the convergence to the stable equilibrium or the coexistence of attractors. We have then performed a detailed analysis of the global dynamic phenomena occurring when, by increasing the parameter c, the equilibrium O becomes unstable via a Neimark–Hopf bifurcation: we have numerically observed that when this bifurcation occurs at sufficiently high values of the parameter a, an increase of c leads to oscillatory behaviour which may become chaotic around O, and as c approaches the value 1 the dominating state is an attracting cycle (although coexisting with a strange repellor) with a wide basin of attraction. In this global analysis, the theory of *critical curves* and various numerical tools have been extensively used, for example to explain in detail the appearance of chaotic dynamics associated with *homoclinic bifurcations* of fixed points and cycles. Finally, we have considered a stochastic version of the model to demonstrate, at least qualitatively, how the interaction of the deterministic non-linear dynamic phenomena with a simple external noise process, can generate the typical patterns of financial markets such as volatility clustering, fat tails, peaked return distributions and skewness.

Future developments of the model introduced here would be to analyse the dynamics of the three-dimensional map which arises when the dynamics of the market for the alternative asset is also taken into account (as discussed briefly in Section 3). It is also important to focus on attempts of each group to learn about their economic environment in the face of stochastic factors. Finally, in order to focus on the dynamics induced by the interaction of fundamentalists and the speculative behaviour within a two-dimensional map, we have left in the background the dynamics of the wealth of the two groups. This is perhaps justifiable in the present context since an exponential utility of wealth function underlies both the fundamentalist and chartist demand functions, which in this case are independent of wealth. Clearly, in the long term, the evolution of the wealth of each group will also determine their economic behaviour, and such evolution needs to be modelled. Chiarella and He (2001b) have developed a model of heterogeneous agents with logarithmic utility function which takes explicit account of the wealth dynamics of each group, but the analysis of this model is only possible via computer simulations. However the insights into the

dynamics of speculative behaviour gained via the simpler model of this paper are useful in attempting to understand the dynamics of this more complete model as well as that of Chen and Yeh.

Acknowledgements

This work has been performed with the financial support of CNR, Italy, and within the scope of the national research project "Non-linear Dynamics and Stochastic Models in Economics and Finance", MURST, Italy. Financial support of the Australian Research Council Grant number A79802872 is also acknowledged. We would like to thank the two anonymous referees for helpful comments and Gian Italo Bischi for having read a previous version of this paper, pointing out some misconceptions. We are particularly grateful to Richard Day, whose suggestions have led to major improvements. The usual caveat applies.

References

Beja, A., Goldman, M.B., 1980. On the dynamic behavior of prices in disequilibrium. Journal of Finance 35, 235–248.

Brock, W., Hommes, C., 1998. Heterogeneous beliefs and routes to chaos in a simple asset pricing model. Journal of Economic Dynamics and Control 22, 1235–1274.

Chen, S.H., Yeh, C.H., 1997. Modelling speculators with genetic programming. In: Angeline, P., et al. (Eds.), Evolutionary Programming VI, Lecture Notes in Computer Science, Vol. 1213, Springer, Berlin, pp. 137–147.

Chiarella, C., 1992. The dynamics of speculative behaviour. Annals of Operations Research 37, 101–123.

Chiarella, C., Dieci, R., Gardini, L., 2001a. A dynamic analysis of speculation across two markets. Working Paper, School of Finance and Economics, University of Technology, Sydney, Australia.

Chiarella, C., Dieci, R., Gardini, L., 2001b. Asset price dynamics in a financial market with fundamentalists and chartists. Discrete Dynamics in Nature and Society 6, 69–99.

Chiarella, C., He, X., in press. Heterogeneous beliefs, risk and learning in a simple asset pricing model. Computational Economics.

Chiarella, C., He, X., 2001. Asset Pricing and Wealth Dynamics under Heterogeneous Expectations. Quantitative Finance 1, 509–526.

Collet, P., Eckmann, J.P., 1980. Iterated Maps on the Interval as Dynamical Systems, Birkhauser, Basel, Boston.

Day, R.H., Huang, W., 1990. Bulls, bears and market sheep. Journal of Economic Behavior and Organization 14, 299–329.

Devaney, R.L., 1987. An Introduction to Chaotic Dynamical systems, The Benjamin/Cummings Publishing Co., Menlo Park, CA.

Gardini, L., 1994. Homoclinic bifurcations in n-dimensional endomorphisms due to expanding periodic points. Non-linear Analysis, T.M.&A. 23, 1039–1089.

Gumowski, I., Mira, C., 1980. Dynamique Chaotique. Cepadues, Toulouse.

Li, T.Y., Yorke, J.A., 1975. Period three implies chaos. American Mathematical Monthly 82, 985–992.

Lux, T., 1998. The socio-economic dynamics of speculative markets: interacting agents, chaos and the fat tails of return distributions. Journal of Economic Behaviour and Organization 33, 143–165.

Marotto, F.R., 1978. Snap-back repellers imply chaos in $\boldsymbol{R}^n$. Journal of Mathematical Analysis and Applications 72, 199–223.

Mira, C., 1987. Chaotic Dynamics, World Scientific, Singapore.

Mira, C., Gardini, L., Barugola, A., Cathala, J.C., 1996. Chaotic Dynamics in Two-Dimensional Non-invertible Maps, World Scientific, Singapore.

Puu, T., 2000. Attractors, Bifurcations and Chaos. Springer, New York.

Zeeman, E.C., 1974. On the unstable behaviour of stock exchanges. Journal of Mathematical Economics 1, 39–49.